Synthesis and Biological Evaluation of Organoruthenium Complexes with Azole Antifungal Agents. First Crystal Structure of a Tioconazole Metal Complex

ARTICLE *in* ORGANOMETALLICS · MARCH 2014

Impact Factor: 4.13 · DOI: 10.1021/om401096y

5 AUTHORS, INCLUDING:

Jakob Kljun
Faculty of Chemistry and Chemical Technolog…
22 PUBLICATIONS **354** CITATIONS
SEE PROFILE

Tea Lanisnik Rizner
University of Ljubljana
113 PUBLICATIONS **1,739** CITATIONS
SEE PROFILE

ORGANOMETALLICS

Article

pubs.acs.org/Organometallics

Synthesis and Biological Evaluation of Organoruthenium Complexes with Azole Antifungal Agents. First Crystal Structure of a Tioconazole Metal Complex

Jakob Kljun,[†,‡] Antony James Scott,[§] Tea Lanišnik Rižner,[⊥] Jennifer Keiser,[∥,#] and Iztok Turel*[,†,‡]

[†]Faculty of Chemistry and Chemical Technology, University of Ljubljana, Aškerčeva 5, SI-1000 Ljubljana, Slovenia

[‡]EN→FIST Centre of Excellence, Dunajska 156, SI-1000 Ljubljana, Slovenia

[§]The University of Glasgow, University Avenue, Glasgow G12 8QQ, Scotland, U.K.

[⊥]Institute of Biochemistry, Faculty of Medicine, University of Ljubljana, Vrazov trg 2, SI-1000 Ljubljana, Slovenia

[∥]Department of Medical Parasitology and Infection Biology, Swiss Tropical and Public Health Institute, P.O. Box, CH−4002 Basel, Switzerland

[#]University of Basel, P.O. Box, CH−4003 Basel, Switzerland

Supporting Information

ABSTRACT: Nine organoruthenium complexes with azole antifungal agents (L) clotrimazole (**ctz**), tioconazole (**tcz**), and miconazole (**mcz**) with the general formulas [(η^6-*p*-cymene)-$RuCl_2(L)$], [(η^6-*p*-cymene)$RuCl(L)_2$]Cl, and [(η^6-*p*-cymene)-$Ru(L)_3$]$(PF_6)_2$ were prepared and characterized by NMR, HRMS, IR, UV−vis, and X-ray crystallography. Herein, we report the first crystal structure of a tioconazole metal complex as well as the structure of the tioconazole ligand itself and the bis-clotrimazole complex as a hexafluorophosphate salt. The complexes possess a pseudooctahedral geometry typical for organoruthenium(II) compounds where half of the coordination sites are occupied by the π-bonded arene ligand *p*-cymene while the remaining sites are occupied by either the chlorido ligands and/or the azole ligands. The stability of the compounds in dmso solution was studied by NMR spectroscopy. The biological activity of all nine complexes and the ruthenium precursor against the fungus *Culvularia lunata* was evaluated. The complexes showed antifungal activity at low millimolar concentrations, where the activity decreased with the increasing number of ligands. However at 0.5 mM concentrations all tris-azole complexes statistically significantly reduced the radial growth rate, and also at 0.01 mM concentrations the monoazole complexes showed statistically significant effects. **Mcz** and its complexes were also tested against the human parasite *Schistosoma mansoni* and revealed schistocidal activity at 10−100 μg/mL in vitro.

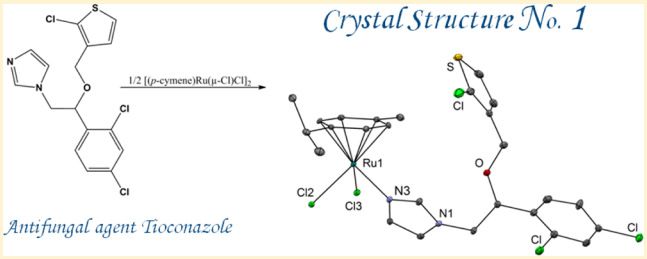

INTRODUCTION

Azole-type molecules are known sterol biosynthesis inhibitors, which prevent the growth of certain fungi and parasites by inhibiting the cytochrome P-450-dependent C-14-α demethylation of lanosterol to ergosterol and cholesterol, respectively (which are both essential components of their cell membranes).[1] Many of them were and some still are in clinical use, mostly as antifungal agents.

A recurring concept in bioinorganic chemistry is the search for synergism by combining a metal ion containing moiety and a bioactive ligand.[2] It has been proposed that binding of the metal ion, even when the active site of the ligand seems thus blocked, can produce positive effects on the biological activity through various effects: different modes of action, increased absorption, higher solubility, and even changed biological activity. Our group has previously studied the biological properties of organoruthenium complexes of antibacterial agents of the quinolone family and found out that in some cases the antibacterial potency of the complex is not significantly altered, while some of the complexes possess discrete toxicity against certain cancer cell lines and inhibit the activity of cathepsins, which are enzymes that are involved in various pathological processes including cancer.[3,4] Recently, two series of novel ruthenium complexes bearing the azole antifungal agents clotrimazole[5] and ketoconazole[6] were prepared by the group of R. A. Sanchez-Delgado, and their potential as antiparasitic agents against *L. major* and *T. cruzi*, which are the cause of severe ailments such as leishmaniasis and Chagas disease, was evaluated. It is known that ruthenium complexes are active against various microorganisms that cause tropical diseases,[7] and also the organoruthenium complex with ofloxacin, prepared by our group, displayed a modest activity in such tests.[4] It was found by R. A. Sanchez-Delgado that among

Received: November 13, 2013
Published: March 18, 2014

   dx.doi.org/10.1021/om401096y | *Organometallics* 2014, 33, 1594−1601

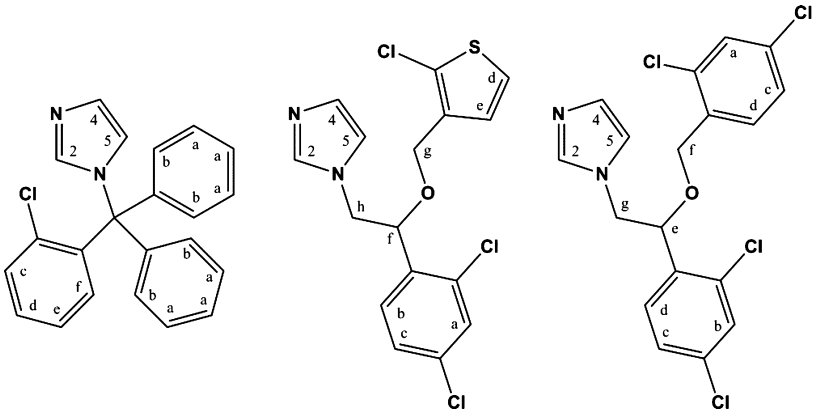

Figure 1. The imidazole antifungals used in our study—(from left to right) clotrimazole (**ctz**), tioconazole (**tcz**), and miconazole (**mcz**)—with the atom numbering used in the assignment of the NMR peaks.

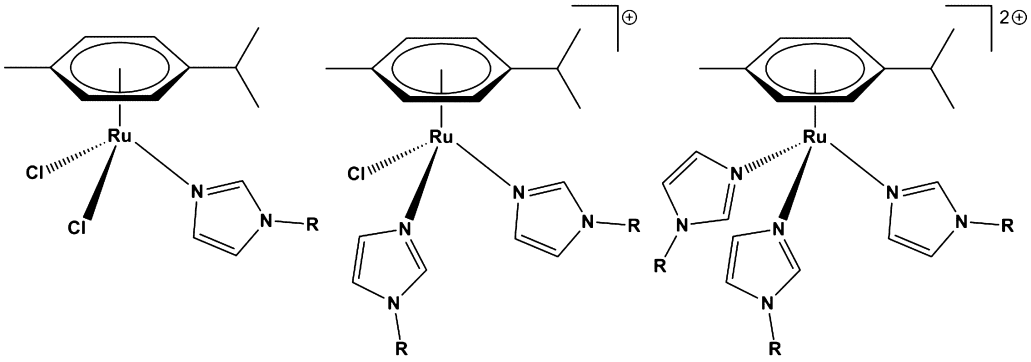

Figure 2. General formulas of the mono-, bis-, and tris-azole organoruthenium species in which the azole ligands are bonded through the N3 imidazole nitrogen atom. In the case of the bis- and tris-complexes of **tcz** and **mcz** the products are mixtures of diastereomers due to the racemic nature of the ligands.

various complexes the organoruthenium species bearing the aromatic cymene ligand were the most effective against the two parasites while presenting no relevant toxicity against human cells. Nonorganometallic complexes were the least effective, while substitution of the two chlorido ligands in the organometallic compounds by bidentate ligands such as bipy, acac, or en resulted in a slightly lesser activity against the parasites.

In the last years fungi have become a great global threat to crops, forests, and animals.[8,9] More than 125 million tons of rice, wheat, maize, potatoes, and soybeans are destroyed by fungi every year.[9] As the use of azole-based agricultural chemicals has been associated with the increased number of triazole-resistant fungal species affecting humans[8] and azole-based antifungal drugs used for treatment of human mycoses have serious side effects,[10] new and potent antifungal compounds with different mechanisms of action are urgently needed. Synthesis of ruthenium complexes of the azole ligands was attempted to contribute in this regard.

With this in mind, we have prepared and characterized seven novel ruthenium complexes using three different imidazole antifungals (L = clotrimazole (**ctz**), miconazole (**mcz**), tioconazole (**tcz**); Figure 1) with the general formulas $[(\eta^6\text{-}p\text{-cymene})RuCl_2(L)]$, $[(\eta^6\text{-}p\text{-cymene})RuCl(L)_2]Cl$, and $[(\eta^6\text{-}p\text{-cymene})Ru(L)_3](PF_6)_2$ (Figure 2). During our study, complex $[(\eta^6\text{-}p\text{-cymene})RuCl_2(ctz)]$, reported by Sanchez-Delgado et al.,[5] and complex $[(\eta^6\text{-}p\text{-cymene})RuCl_2(mcz)]$, reported by Gasser et al.,[11] were also prepared; however, a different synthetic procedure was used. Isolation of these complexes facilitated a comparative study to investigate how different antifungal ligands and different metal–ligand ratios may influence the biological properties of the compounds.

On one hand, we wanted to test the antifungal potential of the novel ruthenium compounds, as we were interested to see if blocking the N3 atom results in the loss of the antifungal activity. We selected a model fungal organism, *Curvularia lunata* (*C. lunata*). This darkly pigmented, dematiaceous fungus is a known plant and human pathogen. The plant diseases include leaf blight on *Sorghum*, leaf spot on *Canabis sativa*, and seedling blight on *Saccharum* spp.[12] *C. lunata* is a causative agent of human diseases in both immunocompromised and immunocompetent individuals, such as allergic fungal sinusitis, endocarditis, peritonitis, eumycetoma, keratitis, allergic bronchopulmonary disease, endophthalmitis, optic neuropathy, and disseminated phaeohyphomycosis.[13] There are limited therapeutic options for the treatment of these frequently fatal infections; thus new antimicotics are needed.

On the other hand, due to the promising results of the ruthenium compounds against parasites causing tropical diseases, we have decided to perform the tests for the miconazole complexes (**1c**, **2c**, and **3c**) against the human parasite *Schistosoma mansoni* (*S. mansoni*), which causes schistosomiasis. Schistosomiasis, also known as bilharzia, is the second most devastating parasitic disease after malaria, and according to the World Health Organization,[14] approximately 200 million people are infected, most of them children. The drug of choice is praziquantel, but its widespread use may soon result in resistance. Two vaccines are now in clinical trials,[14] but

dx.doi.org/10.1021/om401096y | *Organometallics* 2014, 33, 1594−1601

there are still questions about their effectiveness. Due to these reasons, the search for new drugs with different mechanisms of actions for the treatment of fungal and parasitic diseases is very important.

MATERIALS AND METHODS

Synthesis and Characterization. All solvents and reagents, including the dimeric ruthenium precursor $[(\eta^6\text{-}p\text{-cymene})\mathrm{Ru}(\mu\text{-}\mathrm{Cl})\mathrm{Cl}]_2$ (**P1**), were purchased from Sigma-Aldrich and used as received.

X-ray diffraction data for all compounds were collected on an Oxford Diffraction SuperNova diffractometer with Mo microfocus X-ray source (Kα radiation, λ = 0.71073 Å) with mirror optics and an Atlas detector. The structures were solved by direct methods implemented in SIR92[15] and refined by a full-matrix least-squares procedure based on F^2 using SHELXL-97.[16] All non-hydrogen atoms were refined anisotropically. The hydrogen atoms were placed at calculated positions and treated using appropriate riding models. The programs Mercury[17] and Platon[18] were used for data analysis and figure preparation. Additional crystallographic data for the crystal structures are given in Table S1 and Figures S1 and S2. The crystal structures of compounds **tcz**, **1b**, and **2a**·$2CH_2Cl_2$ have been submitted to the CCDC and have been allocated the deposition numbers CCDC 971363−5 for **tcz**, **1b**, and **2a**, respectively.

UV−vis spectra were measured with Perkin-Elmer Lambda 750 UV/vis/NIR spectrometer over a range of 250 to 800 nm (Figures S3−5). ^{1}H NMR spectra were measured with a Bruker Avance III 500 spectrometer at room temperature. With ^{1}H NMR the spectra standard was set as trimethylsilane (TMS) with chemical shift at 0 ppm. Infrared spectra (ATR) were recorded on a Perkin-Elmer Spectrum 100 FTIR spectrometer. The measurements were made in the range 4000 to 600 cm^{-1}. Elemental analyses were performed on a Perkin-Elmer 204C microanalyser. HRMS were measured on an Agilent 6224 Accurate Mass TOF LC mass spectrometer.

Antifungal Activity Test. The antifungal activities of ligands (**ctz**, **mcz**, **tcz**) and their mono-, bis-, and tris-ruthenium complexes were tested. Solid malt extract agar pH 6.5 was prepared with 0.5 and 0.01 mM (final concentrations) of azole ligands and their complexes in dmso or with dmso only. Solutions of azole ligands and their complexes were freshly prepared and immediately added to cooled melted malt extract agar. The final concentration of dmso in malt extract agar was 1%. Petri dishes were centrally inoculated in triplicates with 5 mm mycelia disks taken from 72 h old agar culture of the fungus *C. lunata*. The inoculated plates were then incubated at 26 °C, and the growth of the inoculated mycelia was measured over the following week. The diameter of fungal growth was plotted as a function of time, and the radial growth rate was obtained by linear regression (GraphPad Prism 5).[19]

Antischistosomal Activity Test. Adult *S. mansoni* were collected from the hepatic portal veins and mesenteric veins of infected NMRI mice 7−8 weeks postinfection. Freshly harvested schistosomes were placed in RPMI culture medium supplemented with 5% heat-inactivated fetal calf serum (iFCS), penicillin (100 U/mL), and streptomycin (100 μg/m), quickly rinsed, and stored at 37 °C, 5% CO_2 until usage. The miconazole complexes **1**−**3c** were selected for these tests as model compounds, and stock solutions (10 mg/mL) of **1c**, **2c**, and **3c** as well as the ruthenium precursor **P1** were prepared using dmso. Experiments were conducted in duplicate. Three to five adult *S. mansoni* were incubated in 24-flat-bottom-well plates ((BD Falcon, USA) in the presence of 1−100 μg/mL of the test drugs at 37 °C, 5% CO_2. Schistosomes incubated in the presence of blank medium supplemented with the highest concentration of dmso served as control. Seventy-two hours post drug exposure schistosomes were examined phenotypically using a motility scale ranging from 3 (worms active and healthy) to 1 (worms dead) and an inverse microscope (Carl Zeiss, Germany, magnification 80×).

Synthetic Procedures. *Monoazole Complexes with General Formula $[(\eta^6\text{-}p\text{-Cymene})\mathrm{RuCl}_2(\mathrm{L})]$ (**1a**−**c**).* A 40.0 mg (0.065 mmol) amount of **P1** and 2.05 equiv of the azole ligand (0.134 mmol; (a) 46.2 mg **ctz**, (b) 51.9 mg **tcz**, (c) 55.7 mg **mcz**) were dissolved in 30 mL of a MeOH/$CHCl_3$ (1:1) mixture in a round-bottom flask. The color quickly turned from red to a light orange. The reaction mixture was stirred until complete dissolution (15−30 min) and then refluxed for 30 min, during which the solution became a deeper orange. The reaction mixture was cooled to room temperature and stirred for an additional 4 h, during which time the solution became a deep orange. The solvent mixture was rotary-evaporated. The orange oily residue was dissolved in CH_2Cl_2, the solvent was rotary-evaporated, and the procedure was repeated again twice to remove traces of $CHCl_3$ or MeOH. A concentrated CH_2Cl_2 solution of the complex was then placed in an ice bath for 10 min, and 15−20 mL of cold *n*-hexane was added to produce an orange solid. The product was filtered, washed twice with 2 mL of *n*-hexane, left to dry for 5 min on the vacuum filtration device, and placed in a heater for 3 h at 45 °C (yield: 65 mg, 75% **1a**; 64 mg, 68% **1b**; 68 mg, 71% **1c**).

*$[(\eta^6\text{-}p\text{-Cymene})\mathrm{RuCl}_2(\mathrm{ctz})]$ (**1a**).* ^{1}H NMR ($CDCl_3$, 500.10 MHz): δ 7.83 (t, 1H, J = 1.3 Hz, *H2* ctz), 7.45 (dd, 1H, J = 7.9, 1.4 Hz, H_c ctz), 7.38 (dd, 1H, J = 7.5, 1.5 Hz, H_d ctz), 7.35 (dd, 7H, J = 4.2, 2.2 Hz, H_a, *H4* ctz), 7.29 (dd, 1H, J = 7.9, 1.3 Hz, H_e ctz), 7.15−7.09 (m, 4H, H_b ctz), 7.01 (dd, 1H, J = 8.0, 1.5 Hz, H_f ctz), 6.82 (t, 1H, J = 1.7 Hz, *H5* ctz), 5.31 (d, 2H, J = 6.0 Hz, Ar-*H* cym), 5.12 (d, 2H, J = 5.9 Hz, Ar-*H* cym), 2.86 (dq, 1H, J = 13.8, 7.0 Hz, Ar-C*H*-$(CH_3)_2$, cym), 2.09 (s, 3H, Ar-CH_3 cym), 1.19 (d, 6H, J = 6.9 Hz, Ar-CH-$(CH_3)_2$ cym) ppm. Selected IR bands (cm^{-1}, ATR): 3499, 2959, 1445, 1492, 1220, 1042, 1087, 750, 709. UV−vis (λ [nm], ε [L mol^{-1} cm^{-1}] for $c = 1 \times 10^{-3}$ M, MeOH): 328.5 (1166.0), 406.2 (672.2). HRMS-ESI (m/z): $[M - Cl]^+$ calcd for $C_{32}H_{31}Cl_2N_2Ru$ 615.0908, found 615.0906. Anal. Calcd for $C_{32}H_{31}Cl_3N_2Ru$: C, 59.04; H, 4.80; N, 4.30. Found: C, 58.84; H, 4.80; N, 4.32.

*$[(\eta^6\text{-}p\text{-Cymene})\mathrm{RuCl}_2(\mathrm{tcz})]$ (**1b**).* ^{1}H NMR ($CDCl_3$, 500.10 MHz): δ 7.87 (s, 1H, *H2* tcz), 7.43 (d, 1H, J = 1.9 Hz, *Ha* tcz), 7.34 (d, 1H, J = 8.4 Hz, H_b tcz), 7.30 (dd, 1H, J = 8.4, 1.9 Hz, H_c tcz), 7.26 (s, 1H, CDCl, *H4* tcz, overlapping with solvent peak), 7.12 (d, 1H, J = 5.7 Hz, H_d tcz), 6.91 (d, 1H, J = 5.7 Hz, H_e tcz), 6.84 (t, 1H, J = 1.4 Hz, *H5* tcz), 5.39 (dd, 2H, J = 5.3, 2.6 Hz, Ar-*H* cym), 5.19 (d, 2H, J = 5.9 Hz, Ar-*H* cym), 4.93 (dd, 1H, J = 7.5, 2.8 Hz, H_f tcz), 4.40 (d, 1H, J = 11.8 Hz, H_g tcz), 4.27 (d, 1H, J = 11.8 Hz, H_g tcz), 4.10 (dd, 1H, J = 14.5, 2.8 Hz, H_h tcz), 3.98 (dd, 1H, J = 14.5, 7.6 Hz, H_h tcz), 2.96 (hept, 1H, J = 6.9 Hz, Ar-C*H*-$(CH_3)_2$, cym), 2.14 (s, 3H, Ar-CH_3 cym), 1.28 (d, 6H, J = 6.9, 1.7 Hz, Ar-CH-$(CH_3)_2$ cym). Selected IR bands (cm^{-1}, ATR): 3674, 3072, 3039, 2959, 2870, 1525, 1467, 1238, 1382, 1089, 1028, 823, 746, 657. UV−vis (λ [nm], ε [L mol^{-1} cm^{-1}] for $c = 1 \times 10^{-3}$ M, MeOH): 327.1 (1070.0), 408.7 (636.6). HRMS-ESI (m/z): $[M - Cl]^+$ calcd for $C_{26}H_{27}Cl_4N_2ORuS$ 658.9612, found 658.9620. Anal. Calcd for $C_{26}H_{27}Cl_5N_2ORuS$: C, 45.00; H, 3.92; N, 4.04. Found: C, 45.33; H, 4.07; N, 3.97.

*$[(\eta^6\text{-}p\text{-Cymene})\mathrm{RuCl}_2(\mathrm{mcz})]$ (**1c**).* ^{1}H NMR ($CDCl_3$, 500.10 MHz): δ 7.91 (s, 1H, *H2* mcz), 7.45 (d, 1H, J = 0.9 Hz, H_a mcz), 7.38 (d, 1H, J = 4.4 Hz, H_b mcz), 7.36−7.33 (m, 2H, H_c mcz), 7.30 (d, 2H, J = 1.7 Hz, H_d mcz), 7.27 (s, 1H, *H4* mcz, overlapping with solvent peak), 6.84 (s, 1H, *H5* mcz), 5.39 (d, 2H, J = 5.7 Hz, Ar-*H* cym), 5.20 (d, 2H, J = 5.2 Hz, Ar-*H* cym), 5.02 (dd, 1H, J = 7.4, 2.8 Hz, H_e mcz), 4.48 (d, 1H, J = 12.3 Hz, H_f mcz), 4.37 (d, 1H, J = 12.3 Hz, H_f mcz), 4.16 (dd, 1H, J = 14.6, 2.8 Hz, H_g mcz), 4.06 (dd, 1H, J = 14.6, 7.4 Hz, H_g mcz), 2.95 (m, 1H, Ar-C*H*-$(CH_3)_2$, cym), 2.15 (s, 3H, Ar-CH_3 cym), 1.26 (d 6H, J = 6.9 Hz, Ar-CH-$(CH_3)_2$ cym) ppm. Selected IR bands (cm^{-1}, ATR): 3667, 2971, 2901, 1561, 1471, 1250, 1090, 1044, 864, 789. UV−vis (λ [nm], ε [L mol^{-1} cm^{-1}] for $c = 1 \times 10^{-3}$ M, MeOH): 327.5 (1089.3),406.6 (648.6). HRMS-ESI (m/z): $[M - Cl]^+$ calcd for $C_{28}H_{28}Cl_5N_2ORu$ 686.9658, found 686.9663. Anal. Calcd for $C_{28}H_{28}Cl_6N_2ORu$: C, 46.56; H, 3.91; N, 3.88. Found: C, 46.30; H, 3.72; N, 4.01.

*Bis-azole Complexes with General Formula $[(\eta^6\text{-}p\text{-Cymene})\mathrm{RuCl}(\mathrm{L})_2]\mathrm{Cl}$ (**2a**−**c**).* A 40.0 mg (0.065 mmol) amount of **P1** and 4.10 equiv of the azole ligand (0.2678 mmol; (a) 92.4 mg **ctz**, (b) 103.9 mg **tcz**, (c) 111.5 mg **mcz**) were dissolved in 30 mL of a MeOH/$CHCl_3$ (1:1) mixture in a round-bottom flask. The color of the reaction mixture turned from red to a light yellow. The reaction mixture was stirred until complete dissolution (15−30 min) and then refluxed for 5 h,

dx.doi.org/10.1021/om401096y | *Organometallics* 2014, 33, 1594−1601

during which the solution became yellow. The solvent mixture was rotary-evaporated. The orange oily residue was dissolved in CH_2Cl_2, the solvent was rotary-evaporated, and the procedure was repeated again twice to remove traces of $CHCl_3$ or MeOH. A concentrated CH_2Cl_2 solution of the complex was then placed in an ice bath for 10 min, and 15−20 mL of cold *n*-hexane was added to produce a pale orange solid. The product was filtered, washed twice with 2 mL of *n*-hexane, left to dry for 5 min on the vacuum filtration device, and placed in a heater for 3 h at 45 °C (yield: 118 mg, 89% **2a**; 129 mg, 82% **2b**; 115 mg, 77% **2c**).

[(η^6-p-Cymene)RuCl(ctz)$_2$]Cl (**2a**). ^{1}H NMR ($CDCl_3$, 500.10 MHz): δ 7.89 (s, 2H, *H2* ctz), 7.47 (s, 2H, *Hc* ctz), 7.39 (dd, 2H, *H4* ctz), 7.37 (dd, 2H, H_d ctz), 7.35−7.27 (m, 12H, H_a ctz), 7.22−7.17 (m, 2H, H_e ctz), 6.98−6.92 (m, 8H, H_b, ctz), 6.89−6.86 (m, 2H, H_f ctz), 6.85 (t, 2H, *H5* ctz), 5.69 (d, 2H, Ar-*H* cym), 5.50 (d, 2H, Ar-*H* cym), 2.47 (sept, 1H, Ar-C*H*-$(CH_3)_2$, cym), 1.81 (s, 3H, Ar-CH_3 cym), 1.10 (d, 6H, Ar-CH-(CH_3)$_2$ cym) ppm. Selected IR bands (cm^{-1}, ATR): 3670, 2970, 1446, 1492, 1218, 1087, 836, 749. UV−vis (λ [nm], ε [L mol^{-1} cm^{-1}] for $c = 1 \times 10^{-3}$ M, MeOH): 322.2 (953.8), 395.2 (596.7). HRMS-ESI (m/z): $[M + 2]^+$ calcd for $C_{54}H_{48}Cl_3N_4Ru$: 961.1954, found 961.1976. Anal. Calcd for $C_{54}H_{48}Cl_4N_4Ru$: C, 65.13; H, 4.86; N, 5.53. Found: C, 65.35; H, 4,78; N, 5.37.

[(η^6-p-Cymene)RuCl(tcz)$_2$]Cl (**2b**). ^{1}H NMR ($CDCl_3$, 500.10 MHz): δ 8.05 (d, 1H, *H2* tcz), 7.98 (d, 1H, *H2* tcz), 7.42−7.34 (m, 3H, *Ar-H* tcz), 7.28 (m, 1H, *Ar-H* tcz), 7.25 (m, 4H, *Ar-H* tcz), 7.10 (m, 2H, *Ar-H* tcz), 6.94 (m, 1H, *Ar-H* tcz), 6.80 (m, 2H, *Ar-H* tcz), 6.66 (d, 1H, *Ar-H* tcz), 5.58 (m, 2H, Ar-*H* cym), 5.41 (m, 2H, Ar-*H* cym), 4.94 (dd, 2H, H_f tcz), 4.38−4.07 (m, 8H, $H_{g/h}$ tcz), 2.28 (sept, 1H, Ar-C*H*-$(CH_3)_2$, cym), 1.63 (s, 3H, Ar-CH_3 cym), 1.08 (m, 6H, Ar-CH-(CH_3)$_2$ cym) ppm. Selected IR bands (cm^{-1}, ATR): 3140, 2926, 1522, 1469, 1242, 1088, 1032, 835, 738. UV−vis (λ [nm], ε [L mol^{-1} cm^{-1}] for $c = 1 \times 10^{-3}$ M, MeOH): 320.7 (1009.6), 397.7 (638.3). HRMS-ESI (m/z): $[M + 4]^+$ calcd for $C_{42}H_{40}Cl_7N_4O_2RuS_2$ 1046.9392, found 1046.9418. Anal. Calcd for $C_{42}H_{40}Cl_8N_4O_2RuS_2$: C, 46.64; H, 3.73; N, 5.18. Found: C, 46.29; H, 3.84; N, 4.98.

[(η^6-p-Cymene)RuCl(mcz)$_2$]Cl (**2c**). ^{1}H NMR ($CDCl_3$, 500 MHz): δ 9.12 (dd, 2H, *H2* mcz), 7.61 (d, 2H, Ar-*H* mcz), 7.55 (dd, 2H, Ar-*H* mcz), 7.49−7.16 (m, 10H, Ar-*H* mcz), 6.72 (dd, 2H, Ar-*H* mcz), 5.85−5.69 (m, 4H, Ar-*H* cym), 5.06 (m, 2H, *Hd* mcz), 4.55−4.03 (m, 8H, H_e mcz), 2.30−2.15 (m, 1H, Ar-C*H*-$(CH_3)_2$, cym), 1.59 (d, 3H, Ar-CH_3 cym), 1.02 (m, 6H, Ar-CH-(CH_3)$_2$ cym) ppm. Selected IR bands (cm^{-1}, ATR): 3144, 2973, 2901, 1589, 1471, 1244, 1092, 1044, 838, 740. UV−vis (λ [nm], ε [L mol^{-1} cm^{-1}] for $c = 1 \times 10^{-3}$ M, MeOH): 321.1 (1011.0), 398.8 (652.3). HRMS-ESI (m/z): $[M + 4]^+$ calcd for $C_{46}H_{42}Cl_9N_4O_2Ru$ 1102.9489, found 1102.9494. Anal. Calcd for $C_{46}H_{42}Cl_{10}N_4O_2Ru$: C, 48.53; H, 3.72; N, 4.92. Found: C, 48.41; H, 3.97; N, 4.73.

Tris-azole Complexes with General Formula [(η^6-p-Cymene)Ru-(L)$_3$](PF$_6$)$_2$ (**3a−c**). A 40.0 mg (0.0663 mmol) amount of **P1** and 6.15 equiv of the azole ligand (0.4017 mmol; (a) 138.5 mg **ctz**, (b) 155.7 mg **tcz**, (c) 167.2 mg **mcz**) were dissolved in 30 mL of a MeOH/$CHCl_3$ (1:1) mixture in a brown round-bottom flask. Soon after dissolution the color turned from red to yellow. A 68.7 mg (0.272 mmol, 4.10 equiv) amount of $AgPF_6$ was added, and the reaction mixture was refluxed for 3 h, during which the solution became a very pale yellow. The solvent was evaporated and the oily residue dissolved in CH_2Cl_2. The precipitate AgCl was filtered over Celite, and the mother solution was evaporated. The dark yellow oily residue was dissolved in CH_2Cl_2, the solvent was rotary-evaporated, and the procedure was repeated again twice to remove traces of $CHCl_3$ or MeOH. A concentrated CH_2Cl_2 solution of the complex was then placed in an ice bath for 10 min, and 15−20 mL of cold *n*-hexane was added to produce a yellow solid. The product was filtered with a vacuum filtration apparatus, washed twice with 2 mL of *n*-hexane, left to dry for 5 min on the vacuum filtration device, and placed in a heater for 3 h at 45 °C (yield: 179 mg, 86% **3a**; 181 mg, 80% **3b**; 197 mg, 83% **3c**).

[(η^6-p-Cymene)Ru(ctz)$_3$](PF$_6$)$_2$ (**3a**). ^{1}H NMR ($CDCl_3$, 500.10 MHz): δ 7.53 (s, 3H, *H2* ctz), 7.35−7.20 (m, 27H, Ar-*H* ctz), 7.03−6.98 (m, 6H, Ar-*H* ctz), 6.96 (d, 12H, Ar-*H* ctz), 6.85 (s, 3H. Ar-*H* ctz), 6.21 (d, 2H, Ar-*H* cym), 6.04 (d, 2H, Ar-*H* cym), 2.01 (dt, 1H, Ar-C*H*-$(CH_3)_2$, cym), 1.82 (s, 3H, Ar-CH_3 cym), 0.95 (d, 6H, Ar-CH-(CH_3)$_2$ cym). Selected IR bands (cm^{-1}, ATR): 2972, 2901, 1447, 1493, 1218, 1087, 1049, 835, 749, 710. UV−vis (λ [nm], ε [L mol^{-1} cm^{-1}] for $c = 1 \times 10^{-3}$ M, MeOH): 309.4 (948.6), 380.7 (657.9). HRMS-ESI (m/z): $[M + 2]^{2+}$ calcd for $C_{76}H_{65}Cl_3N_6Ru$ 1270.3350, found 1270.3420. Anal. Calcd for $C_{76}H_{65}Cl_3F_{12}N_6P_2Ru$: C, 58.52; H, 4.20; N, 5.39. Found: C, 58.63; H, 4.37; N, 5.51.

[(η^6-p-Cymene)Ru(tcz)$_3$](PF$_6$)$_2$ (**3b**). ^{1}H NMR ($CDCl_3$, 500.10 MHz): δ 8.14 (d, 3H, *H2* tcz), 7.40 (m, 3H, Ar-*H* tcz), 7.33 (m, 3H, Ar-*H* tcz), 7.26 (overlapping with $CHCl_3$, s, 6H, Ar-*H* tcz), 7.10 (m, 3H, Ar-*H* tcz), 7.02 (m, 3H, Ar-*H* tcz), 6.81 (m, 3H, Ar-*H* tcz), 5.68−5.51 (m, 4H, Ar-*H* cym), 5.06 (d, 3H, H_f tcz), 4.46−4.29 (m, 12H, $H_{g/h}$ tcz), 2.03 (m, 1H, Ar-C*H*-$(CH_3)_2$, cym), 1.48 (s, 3H, Ar-CH_3 cym), 0.97 (m, 6H, Ar-CH-(CH_3)$_2$ cym) ppm. Selected IR bands (cm^{-1}, ATR): 2870, 1526, 1470, 1245, 1096, 836, 739. UV−vis (λ [nm], ε [L mol^{-1} cm^{-1}] for $c = 1 \times 10^{-3}$ M, MeOH): 306.2 (914.8), 380.3 (665.4). HRMS-ESI (m/z): $[M + 4]^{2+}$ calcd for $C_{58}H_{53}Cl_9N_6O_3RuS_3$ 1397.9523, found 1397.9566. Anal. Calcd for $C_{58}H_{53}Cl_9F_{12}N_6O_3P_2RuS_3$: C, 41.26; H, 3.16; N, 4.98. Found: C, 41.11; H, 3.37; N, 4.79.

[(η^6-p-Cymene)Ru(mcz)$_3$](PF$_6$)$_2$ (**3c**). ^{1}H NMR ($CDCl_3$, 500.10 MHz): δ 8.19−8.11 (m, 3H, *H2* mcz), 7.57−7.42 (m, 3H, Ar-*H* mcz), 7.44−7.27 (m, overlapping with $CHCl_3$, 12H, Ar-*H* mcz), 6.88−6.78 (m, 3H, Ar-*H* mcz), 5.98−5.87 (m, 4H, Ar-*H* cym), 5.64−5.49 (m, 6H, H_d mcz) 5.12 (dt, 3H, H_c mcz), 4.54−4.26 (m, 12H, H_d mcz), 1.96−1.83 (m, 1H, Ar-C*H*-$(CH_3)_2$, cym), 1.39 (s, 3H, Ar-CH_3 cym), 0.90−0.86 (m, 6H, Ar-CH-(CH_3)$_2$ cym) ppm. Selected IR bands (cm^{-1}, ATR): 3146, 2974, 2901, 1523, 1473 1246, 1093, 1044, 838, 740. UV−vis (λ [nm], ε [L mol^{-1} cm^{-1}] for $c = 1 \times 10^{-4}$ M, MeOH): 308.7 (1049.8), 379.9 (778.0). HRMS-ESI (m/z): $[M + 6]^{2+}$ calcd for $C_{64}H_{56}Cl_{12}N_6O_3Ru$ 1483.9631, found 1483.9662. Anal. Calcd for $C_{64}H_{56}Cl_{12}F_{12}N_6O_3P_2Ru$: C, 43.34; H, 3.18; N, 4.74. Found: C, 42.99; H, 3.38; N, 4.61.

RESULTS AND DISCUSSION

Syntheses and Characterization. The three types of complexes were prepared by fairly similar procedures, in which the reaction was carried out in a methanol/chloroform mixture, which offers a high solubility for most organoruthenium precursors and ligands. For the preparation of monoazole compounds, the literature offers various synthetic procedures concerning the choice of solvent (acetone, dichloromethane, toluene), the reaction conditions, and time (1−16 h).[5,20,21] The group of Sanchez-Delgado reports the synthesis of the clotrimazole complex **1a** as a product of a six-hour reaction at room temperature in acetone, followed by the precipitation with Et_2O,[5] while Gasser et al.[11] reported the synthesis of the monomiconazole complex **1c** as a result of a prolonged 20 h reaction in acetone. We discovered that the use of acetone in our case was not suitable, since the monoazole compounds were found to decompose over time, resulting in darker, brown solutions, which required purification. The decomposition was avoided by refluxing the MeOH/$CHCl_3$ reaction mixture for 30 min, which jump-started the reaction. The reaction mixture was then stirred until the completion of the reaction, which was monitored by TLC. Generally the reactions were complete after about 2 h, but occasionally additional stirring up to 4 h was necessary. Moreover, compound **1c** was not fully characterized, as it was reported as unstable in solvents commonly used in NMR spectroscopy. We have found that some organo-ruthenium-azole complexes are indeed unstable in solution; however the compounds can be stabilized for a period of time by using fresh deuterated solvents and avoiding exposure to direct sunlight. The photostability of the complexes was not

dx.doi.org/10.1021/om401096y | *Organometallics* 2014, 33, 1594−1601

evaluated; however the photoinduced release of monodentate nitrogen ligands was observed in the case of structurally similar (organo)ruthenium complexes[22] with a rate and speed that are strongly dependent on the ruthenium coordination sphere.

Crystallizations were attempted by slowly evaporating the compound solutions in solvent mixtures containing a chlorinated solvent, in which the compounds are well soluble (CH_2Cl_2, $CHCl_3$), and nonpolar solvents such as *n*-hexane, cyclohexane, *n*-heptane, or toluene. Crystals of compound **1b** were obtained by the slow evaporation of a CH_2Cl_2/*n*-hexane mixture, and herein we report the first crystal structure of a tioconazole metal complex as well as the crystal structure of the azole ligand itself.

Bis-azole ruthenium complexes were previously reported by Dyson and Vock in two articles, one with substituted imidazoles and one with anthracene- or phenoxazine-functionalized ligands.[20,21] These syntheses were carried out in methanol, 2-propanol, or *n*-butanol at elevated temperatures and with 2-fold excess of the ligand, which was needed to be later removed by extraction using ethyl acetate. In our case the use of a methanol/chloroform mixture needed only a slight excess (2−3%) of the ligand and no further purification. In order to obtain crystals suitable for X-ray diffraction, analogous compounds containing different counterions were prepared by the addition of 10−20 molar equiv of the appropriate salt ($NaBF_4$, KPF_6, $NaBPh_4$) to the initial reaction mixture and subsequent filtration of the precipitated inorganic salts from a CH_2Cl_2 solution. In the case of complex **2a**, [(η^6-*p*-cymene)-$RuCl(ctz)_2$](PF_6) crystals were obtained by the slow evaporation of a CH_2Cl_2/*n*-hexane solution.

The synthesis of the tris-azole complexes required the use of silver salts in order to remove the chlorido ligands from the reaction mixture, as even the use of 20 molar equiv of the azole ligands affords the bis-azole complexes as proven by NMR spectra (Figure 3).

Due to the racemic nature of the **tcz** and **mcz** ligands, complexes **2b**, **2c**, **3b**, and **3c** are mixtures of diastereomers/enantiomers that can be seen in the NMR spectra, as the multiplets are less defined (Figures S6−14). The purity of the compounds was thus further assessed by elemental analyses and high-resolution mass spectrometry.

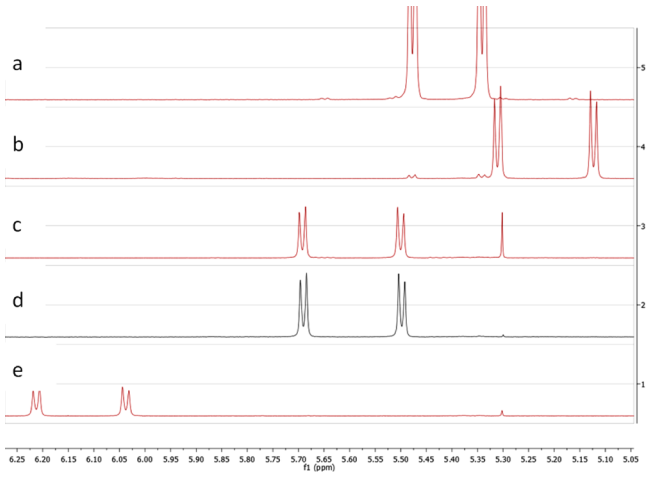

Figure 3. ^{1}H NMR spectra (in $CDCl_3$) in the region pertaining to the aromatic protons of the ruthenium-bound cymene ligand: (a) ruthenium precursor **P1**, (b) compound **1a**, (c) compound **2a**, (d) product of the reaction between the precursor **P1** and 20 molar equiv of **ctz**, (e) compound **3a**, synthesized using the silver salt $AgPF_6$.

Early studies by Vock et al.[21] do not report any issues concerning the stability of structurally similar complexes in aqueous media while performing biological assays; however, Gasser et al.[11] recently demonstrated that dissolution of organoruthenium complexes bearing one monodentate nitrogen ligand (with general formula [(η^6-*p*-cymene)Ru(*N*-ligand)-Cl_2]) can induce the precipitation of the ligand and formation of the [(η^6-*p*-cymene)Ru(*S*-dmso)Cl_2] species. Interestingly, parallel cytotoxicity experiments have shown that organoruthenium complexes bearing one nitrogen ligand show remarkably similar cytotoxic effects to the combination of the ruthenium-dmso adduct and the free ligand in 1:1 ratio, which are, however, inactive if applied separately. Since our compounds have relatively low aqueous solubility and biological experiments were performed by diluting concentrated dmso stock solutions with water in order to obtain the desired concentrations, the stability of the complexes in soliution was investigated. Our studies confirm that the monoazole compounds indeed partially dissociate in dmso, resulting in a mixture of the monoazole- and dmso-ruthenium species. The bis- and tris-azole complexes however appear stable in dmso and aqueous solution with a minority (<3%) of decomposition products appearing after 12 h (Figures S15−18).

Crystal Structures. The crystals of complex **1b** were obtained by slow evaporation of the CH_2Cl_2/*n*-hexane (1:1) solution, which afforded dark yellow needles. So far, this is the first reported tioconazole metal complex. Complex **2a** was crystallized as a hexafluorophosphate salt. Crystals were obtained by the slow evaporation of the CH_2Cl_2/*n*-hexane (1:1) solution, which afforded orange needles. Crystals of the ligand **tcz** were obtained by the slow evaporation of the chloroform solution. Crystals of complexes **1b** and **2a** were unstable in air due to the presence of volatile solvent molecules in the crystal structure. In the case of **2a**, two dichloromethane molecules could be located from the Fourier electron density map, while in the case of **1b** the disorder was too severe and the residual electron density was removed using the SQUEEZE routine within Platon. The software found a solvent-accessible void of 310 Å^3 and with the electron count of 61, which roughly corresponds to two dichloromethane molecules.

The crystal structure of ligand **tcz** (Figure 4) does not present any strong intermolecular interactions (H-bonds, π-stacking). However, a weak hydrogen bond between an aromatic hydrogen on the dichloro-substituted phenyl group and the thienyl sulfur of the adjacent molecule is observed. This S···H distance has a value of 2.81(1) Å, which is considerably smaller than the sum of the van der Waals radii of the two atoms (3.00 Å). The interaction is further confirmed by the near coplanarity of the thienyl and dichlorophenyl moieties (φ = 0.69°) (Figure S1).

The structure of compound **1b** (Figure 5) presents a ruthenium complex with a pseudooctahedral "piano-stool" geometry with the aromatic *p*-cymene ligand π-coordinated to the ruthenium(II) ion. The coordination sphere is completed with two chlorido ligands and the tioconazole ligand, which is bound to ruthenium through the imidazole nitrogen atom N3. The molecules link into dimers about an inversion center by two pairs of *p*-cymene C−H···Cl hydrogen bonds with H···Cl distances of 2.733(1) and 2.716(1) Å, which is considerably less than the sum of van der Waals radii of the two atoms (2.95 Å). The distance between the two ruthenium ions in the dimer is

dx.doi.org/10.1021/om401096y | *Organometallics* 2014, 33, 1594−1601

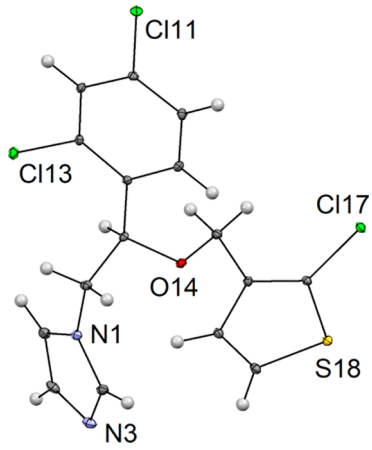

Figure 4. Crystal structure of ligand **tcz** with heteroatom labeling. Thermal ellipsoids are drawn at the 30% probability level.

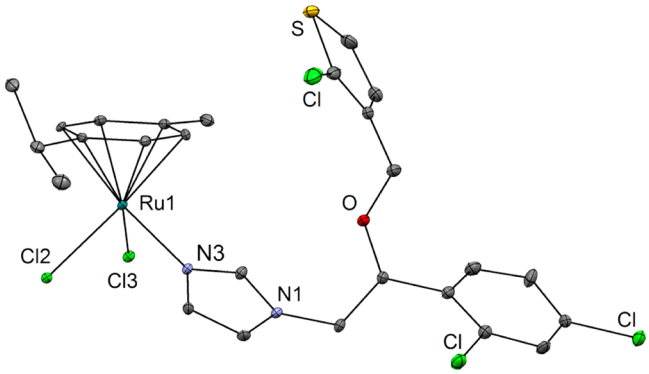

Figure 5. Crystal structure of compound **1b** with heteroatom labeling. Thermal ellipsoids are drawn at the 30% probability level. Hydrogen atoms are omitted for clarity.

5.517(3) Å. The bond lengths and angles are comparable to those from the previously published clotrimazole analogue (Table 1).[5]

Compound **2a** is a cationic organoruthenium complex in which two **ctz** ligands are bonded to the ruthenium ion through the imidazole nitrogen atom N3. A chlorido ligand and the aromatic cymene ring complete the coordination sphere around the metal center with PF_6^- acting as counterion (Figure 6). The complex crystallized with two molecules of dichloromethane, which was used as a solvent in the crystallization process. Addition of a second clotrimazole ligand did not provoke drastic changes in the conformation of the molecule since the bond lengths (Table 1) and angles around the central metal ion remain virtually unchanged. Moreover, in both complexes' crystal structures the coordination to the metal ion did not provoke changes in the bond lengths of the imidazole ring.

Antifungal Activity. The isolated ruthenium complexes showed antifungal activity at low millimolar concentrations. When we followed the effects of the individual azole ligands

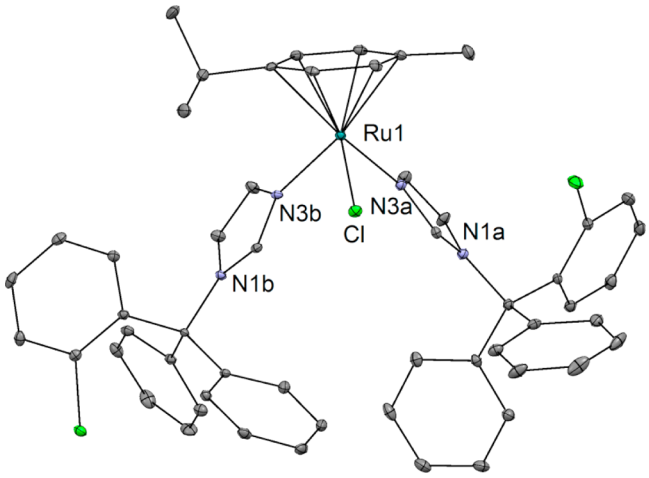

Figure 6. Crystal structure of compound **2a** with heteroatom labeling. Thermal ellipsoids are drawn at the 30% probability level. All hydrogen atoms, the hexafluorophosphate anion, and the cocrystallized solvent molecules are omitted for clarity.

and their mono-, bis-, and tris-ruthenium complexes on the fungal growth, we observed more potent antifungal activity for azole ligands in comparison with their ruthenium complexes (Table 2; Figure S19). Antifungal activities decreased with the

Table 2. Antifungal Activities of Azole Ligands and Their Ruthenium Complexes

	radial growth rate (mm/h)[a]	
compound	0.5 mM	0.01 mM
dmso only	0.36	0.40
ctz	0.01	0.12
1a	0.13	0.30
2a	0.17	0.33
3a	0.16	0.39
mcz	0.04	0.12
1b	0.14	0.17
2b	0.15	0.19
3b	0.19	0.27
tcz	0.04	0.09
1c	0.09	0.15
2c	0.13	0.27
3c	0.13	0.27

[a]Diameters of fungal colonies were measured daily and plotted as a function of time; radial growth rate was calculated by linear regression.

increasing number of ligands in these complexes. However, at 0.5 mM concentrations the tris-ruthenium complexes **3a**−**c** still significantly reduced the radial growth rate by 2.3-, 1.9-, and 2.8-fold, as compared to the control, respectively (Figure S20). Also at 0.01 mM concentrations a 2.3-, 2.4-, and 2.7-fold decline in the growth rate was observed for **1a**−**c**, respectively (Figure S21). Tris-complexes were less potent at 0.01 mM

Table 1. Selected Bond Lengths in the Compounds [(η^6-*p*-cymene)Ru(ctz)Cl_2] (1a), [(η^6-*p*-cymene)Ru(tcz)Cl_2] (1b), and [(η^6-*p*-cymene)Ru(ctz)$_2$Cl](PF_6) (2a)

	1a[5]	1b	2a
Ru−N3	2.098(2)	2.102(4)	2.107(4)/2.111(4)
Ru−Cl	2.412(1)/2.399(1)	2.430(2)/2.421(2)	2.400(2)
Ru−$Cym_{centroid}$	1.664(2)	1.657(2)	1.655(2)

dx.doi.org/10.1021/om401096y | *Organometallics* 2014, 33, 1594−1601

concentrations, but **3b** and **3c** still showed a 1.5-fold decrease in the growth rate.

The azole antifungal compounds inhibit the fungal growth by preventing ergosterol biosynthesis via coordination of their N3 atom to the heme iron within the active site of lanosterol 14α-demethylase.[1] In the mono-, bis-, and tris-azole ruthenium complexes N3 atoms are bound to ruthenium, thus suggesting that the azole ligand complexes inhibit the fungal growth via other mechanisms of action, which may not involve lanosterol 14α-demethylase.[1]

Antischistosomal Activity. No activity was observed following the incubation of adult *S. mansoni* with precursor **P1** for 72 h at a 100 μg/mL concentration (Figure 7). On the other hand the miconazole ligand showed activity at 10 μg/mL following 24 h of incubation and all worms had died (data not shown). Sex-specific activity was documented for compound **3c**: while female worms incubated with 100 μg/mL compound **3c** for 72 h showed only slightly decreased motility, male worms had died. All worms exposed to 100 μg/mL concentration of compounds **1c** and **2c** had died 24–48 h postincubation. Incubation with lower concentrations (1 and 10 μg/mL) of compounds **1c** and **2c** resulted in decreased activities of adult *S. mansoni*. Worms incubated in the presence of dmso (controls) remained active and had a healthy appearance during the entire examination period (Figure 7).

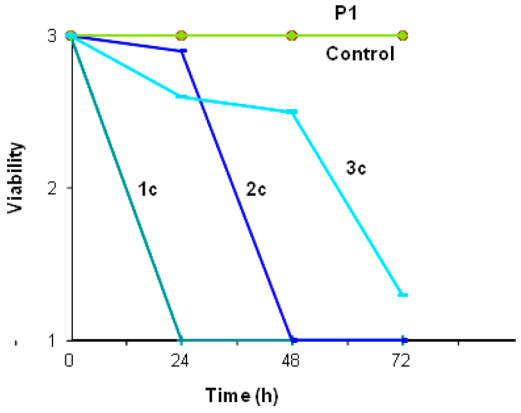

Figure 7. Activity of compounds **1**–**3c** and the ruthenium precursor **P1** against adult *Schistosoma mansoni* at 100 μg/mL over 72 h.

CONCLUSIONS

Organoruthenium complexes of three azole antifungal agents (clotrimazole, miconazole, and tioconazole) were synthesized and evaluated as potential antifungal and antiparasitic agents. For achieving that, optimized synthetic protocols for mono-, bis-, and tris-azole ruthenium complexes were developed that shorten the time and increase the yield as well as the stability of the novel ruthenium-azole complexes. Furthermore, crystal structures of the first tioconazole metal complex, the bis-clotrimazole complex **2a**, and the free **tcz** ligand were determined. Intrigued by the findings of Gasser et al., who reported the deleterious effect of dmso, a commonly used solvent in bioassays, on the stability of [(η^6-*p*-cymene)Ru(azole)Cl_2]) compounds, we explored the stability of our mono-, bis-, and tris-azole complexes in dmso solution. We have found that in our case the monoazole complexes (**1a** and **1b** were also included in the Gasser study[11]) indeed partly decompose, though the decomposition is generally slower than reported, as the equilibrium between the decomposition products is reached in about 12 h. The bis-azole complexes **2a**–**c** and the tris-azole complexes **3a**–**c** are on the other hand stable in dmso solutions, as a minority of decomposition species (<2%) are observed only after 12 h. All in all, the ruthenium complexes statistically significantly reduced the fungal growth rate at 0.5 mM concentration, and the monoazole complexes also did so at 0.01 mM concentrations. In azole ruthenium complexes N3 atoms cannot bind to the heme iron within the active site of lanosterol 14α-demethylase, which suggests a different mechanism of inhibition. The miconazole complexes have shown moderately good antischistosomal activity, which decreases with the number of coordinated azole ligands. However, the gender selectivity displayed by compound **3c** is to the best of our knowledge the first report of such a phenomenon. Given the interesting antischistosomal activities of these compounds, further studies (in vivo studies) should be launched.

ASSOCIATED CONTENT

Supporting Information

Supporting Information contains crystallographic data, UV–vis spectra, ^{1}H NMR spectra, and additional information on antifungal activity tests. This material is available free of charge via the Internet at http://pubs.acs.org.

AUTHOR INFORMATION

Corresponding Author

*E-mail: iztok.turel@fkkt.uni-lj.si.

Notes

The authors declare no competing financial interest.

ACKNOWLEDGMENTS

We are grateful for the financial support from Project J1-4131 and Program Grants P1-0175 (I.T.) and P1-0170 (T.L.R.) and the Junior Researcher Grant for J. Kljun, all funded by the Slovenian Research Agency (ARRS). We thank the EN→FIST Centre of Excellence, Dunajska 156, SI-1000 Ljubljana, for the use of the SuperNova diffractometer. A.J.S. is also grateful for the Erasmus grant, which enabled his 9-month stay in Ljubljana. J. Keiser is financially supported by the Swiss National Science Foundation (SNSF; projects nos. PPOOA-114941 and PPOOP3_135170).

REFERENCES

(1) Sheehan, D. J.; Hitchcock, C. A.; Sibley, C. M. Current and emerging azole antifungal agents. *Clin. Microbiol. Rev.* **1999**, *12*, 40–79.

(2) Turel, I.; Kljun, J. Interactions of metal ions with DNA, its constituents and derivatives, which may be relevant for anticancer research. *Curr. Top. Med. Chem.* **2011**, *11*, 2661–2687. Turel, I. The interactions of metal ions with quinolone antibacterial agents. *Coord. Chem. Rev.* **2002**, *232* (1–2), 27–47.

(3) Hudej, R.; Kljun, J.; Kandioller, W.; Repnik, U.; Turk, B.; Hartinger, C. G.; Keppler, B. K.; Miklavcic, D.; Turel, I. Synthesis and biological evaluation of the thionated antibacterial agent nalidixic acid and its organoruthenium(II) complex. *Organometallics* **2012**, *31*, 5867–5874. Kljun, J.; Bytzek, A. K.; Kandioller, W.; Bartel, C.; Jakupec, M. A.; Hartinger, C. G.; Keppler, B. K.; Turel, I. Physicochemical studies and anticancer potency of ruthenium η^6-*p*-cymene complexes containing antibacterial quinolones. *Organometallics* **2011**, *30*, 2506–2512. Kljun, J.; Bratsos, I.; Alessio, E.; Psomas, G.; Repnik, U.; Butinar, M.; Turk, B.; Turel, I. New uses for old drugs: attempts to convert quinolone antibacterials into potential

anticancer agents containing ruthenium. *Inorg. Chem.* **2013**, *52*, 9039−9052.
(4) Turel, I.; Kljun, J.; Perdih, F.; Morozova, E.; Bakulev, V.; Kasyanenko, N.; Byl, J. A. W.; Osheroff, N. First ruthenium organometallic complex of antibacterial agent ofloxacin. Crystal structure and interactions with DNA. *Inorg. Chem.* **2010**, *49*, 10750−10752.
(5) Martinez, A.; Carreon, T.; Iniguez, E.; Anzellotti, A.; Sanchez, A.; Tyan, M.; Sattler, A.; Herrera, L.; Maldonado, R. A.; Sanchez-Delgado, R. A. Searching for new chemotherapies for tropical diseases: ruthenium-clotrimazole complexes display high in vitro activity against Leishmania major and Trypanosoma cruzi and low toxicity toward normal mammalian cells. *J. Med. Chem.* **2012**, *55*, 3867−3877.
(6) Iniguez, E.; Sanchez, A.; Vasquez, M. A.; Martinez, A.; Olivas, J.; Sattler, A.; Sanchez-Delgado, R. A.; Maldonado, R. A. Metal-drug synergy: new ruthenium(II) complexes of ketoconazole are highly active against Leishmania major and Trypanosoma cruzi and nontoxic to human or murine normal cells. *J. Biol. Inorg. Chem.* **2013**, *18*, 779−790.
(7) Demoro, B.; Sarniguet, C.; Sanchez-Delgado, R.; Rossi, M.; Liebowitz, D.; Caruso, F.; Olea-Azar, C.; Moreno, V.; Medeiros, A.; Comini, M. A.; Otero, L.; Gambino, D. New organoruthenium complexes with bioactive thiosemicarbazones as co-ligands: potential anti-trypanosomal agents. *Dalton Trans.* **2012**, *41*, 1534−1539. Glans, L.; Ehnbom, A.; de Kock, C.; Martinez, A.; Estrada, J.; Smith, P. J.; Haukka, M.; Sanchez-Delgado, R. A.; Nordlander, E. Ruthenium(II) arene complexes with chelating chloroquine analogue ligands: synthesis, characterization and in vitro antimalarial activity. *Dalton Trans.* **2012**, *41*, 2764−2773. Gambino, D.; Otero, L. Perspectives on what ruthenium-based compounds could offer in the development of potential antiparasitic drugs. *Inorg. Chim. Acta* **2012**, *393*, 103−114.
(8) Fisher, M. C.; Henk, D. A.; Briggs, C. J.; Brownstein, J. S.; Madoff, L. C.; McCraw, S. L.; Gurr, S. L. Emerging fungal treats to animal, plant and ecosystem health. *Nature* **2012**, *484*, 186−194.
(9) Kupferschmidt, K. Attack of the clones. *Science* **2012**, *337*, 636−638.
(10) Horvat, S.; Mcwhir, J.; Rozman, D. Defects in cholesterol synthesis genes in mouse and in humans: lessons for drug development and safer treatments. *Drug Metab. Rev.* **2011**, *43*, 69−90.
(11) Patra, M.; Joshi, T.; Pierroz, V.; Ingram, K.; Kaiser, M.; Ferrari, S.; Spingler, B.; Keiser, J.; Gasser, G. DMSO-mediated ligand dissociation: renaissance for biological activity of *N*-heterocyclic-[Ru(η^6-arene)Cl_2] drug candidates. *Chem.—Eur. J.* **2013**, *19*, 14768−14772.
(12) Prom, L. K.; Waniska, R. D.; Kollo, A. I.; Rooney, W. L. Response of eight sorghum cultivars inoculated with *Fusarium thapsinum*, *Curvularia lunata*, and a mixture of the two fungi. *Crop Prot.* **2003**, *22*, 623−628.
(13) Bartynski, J. M.; McCaffrey, T. V.; Frigas, E. Allergic fungal sinusitis secondary to dermatiaceous fungi: *Curvularia lunata* and *Alternaria*. *Otolaryngol.—Head Neck Surg.* **1990**, *103*, 32−39. Travis, W. D.; Kwon-Chung, K. J.; Kleiner, D. E.; Geber, A.; Lawson, W.; Pass, H. I.; Henderson, D. Unusual aspects of allergic bronchopulmonary fungal disease: report of two cases due to *Curvularia* organisms associated with allergic fungal sinusitis. *Hum. Pathol.* **1991**, *22*, 1240−1248. Bryan, C. S.; Smith, C. W.; Berg, D. E.; Karp, R. B. *Curvularia lunata* endocarditis treated with terbinafine: case report. *Clin. Infect. Dis.* **1993**, *16*, 30−32. Lopes, J. O.; Alves, S. H.; Benevenga, J. P.; Brauner, F. B.; Castro, M. S.; Melchiors, E. *Curvularia lunata* peritonitis complicating peritoneal dialysis. *Mycopathologia* **1994**, *127*, 65−67. Janaki, C.; Sentamilselvi, G.; Janaki, V. R.; Devesh, S.; Ajithados, K. Case report. Eumycetoma due to *Curvularia lunata*. *Mycoses* **1999**, *42*, 345−346. Kaushik, S.; Ram, J.; Chakrabarty, A.; Dogra, M. R.; Brar, G. S.; Gupta, A. *Curvularia lunata* endophthalmitis with secondary keratitis. *Am. J. Ophthalmol.* **2001**, *131*, 140−142. Garg, A.; Sujatha, S.; Garg, J.; Parija, S. C.; Thappa, D. M. Eumycetoma due to *Curvularia lunata*. *Indian J. Dermatol. Venereol. Leprol.* **2008**, *74*, 515−516. Wilhelmus, K. R.; Jones, D. B. *Curvularia* keratitis. *Trans. Am. Ophthalmol. Soc.* **2001**, *99*, 111−130. Carter, E.; Boudreaux, C. Fatal cerebral phaeohyphomycosis due to *Curvularia lunata* in an immunocompetent patient. *J. Clin. Microbiol.* **2004**, *2004*, 5419−5423. Smith, T.; Goldschlager, T.; Mott, N.; Robertson, T.; Campbell, S. Optic atrophy due to *Curvularia lunata* mucocoele. *Pituitary* **2007**, *10*, 295−297.
(14) Kupferschmidt, K. A worm vaccine, coming at a snail's pace. *Science* **2013**, *339*, 502−503.
(15) Altomare, A.; Cascarano, G.; Giacovazzo, C.; Guagliardi, A. C.; Burla, M. C.; Polidori, G.; Camalli, M. SIR92−a program for automatic solution of crystal structures by direct methods. *J. Appl. Crystallogr.* **1994**, *27*, 435.
(16) Sheldrick, G. M. A short history of SHELX. *Acta Crystallogr., Sect. A* **2008**, *64*, 112−122.
(17) Macrae, C. F.; Edgington, P. R.; McCabe, P.; Pidcock, E.; Shields, G. P.; Taylor, R.; Towler, M.; van De Streek, J. Mercury: visualization and analysis of crystal structures. *J. Appl. Crystallogr.* **2006**, *39*, 453−457.
(18) Spek, A. L. Structure validation in chemical crystallography. *Acta Crystallogr., Sect. D: Biol. Crystallogr.* **2009**, *65*, 148−155.
(19) Lopez-Malo, A.; Alzamorab, S. M.; Palou, E. *Aspergillus flavus* growth in the presence of chemical preservatives and naturally occurring antimicrobial compounds. *Int. J. Food Microbiol.* **2005**, *99*, 119−128.
(20) Vock, C. A.; Ang, W. H.; Scolaro, C.; Phillips, A. D.; Lagopoulos, L.; Juillerat-Jeanneret, L.; Sava, G.; Scopelliti, R.; Dyson, P. J. Development of ruthenium antitumor drugs that overcome multidrug resistance mechanisms. *J. Med. Chem.* **2007**, *50*, 2166−2175.
(21) Vock, C. A.; Scolaro, C.; Philips, A. D.; Scopelliti, R.; Sava, G.; Dyson, P. J. Synthesis, characterization, and in vitro evaluation of novel ruthenium(II) η^6-arene imidazole complexes. *J. Med. Chem.* **2006**, *49*, 5552−5561.
(22) Betanzos-Lara, S.; Salassa, L.; Habtemariam, A.; Novakova, O.; Pizarro, A. M.; Clarkson, G. J.; Liskova, B.; Brabec, V.; Sadler, P. J. Photoactivatable organometallic pyridyl ruthenium(II) arene complexes. *Organometallics* **2012**, *31*, 3466−3479. Ragazzon, G.; Bratsos, I.; Alessio, E.; Salassa, L.; Habtemariam, A.; McQuitty, R. J.; Clarkson, G. J.; Sadler, P. J. Design of photoactivatable metallodrugs: selective and rapid light-induced ligand dissociation from half-sandwich [Ru([9]aneS_3)(N-N′)(py)]^2 complexes. *Inorg. Chim. Acta* **2012**, *393*, 230−238. Finazzi, I.; Bratsos, I.; Gianferrara, T.; Bergamo, A.; Demitri, N.; Balducci, G.; Alessio, E. Photolabile RuII half-sandwich complexes suitable for developing "caged" compounds: chemical investigation and unexpected dinuclear species with bridging diamine ligands. *Eur. J. Inorg. Chem.* **2013**, *27*, 4743−4753.